Electrical resistivity and equation of state measurements on hot expanded aluminum in the metal-nonmetal transition range

V. N. Korobenko and A. D. Rakhel*
Institute for High Energy Densities, Izhorskaya 13/19, Moscow 125412, Russia
(Received 12 October 2006; revised manuscript received 28 December 2006; published 21 February 2007)

Measurements have been performed on aluminum that expanded from the initial solid state by a factor of 6–9 under a supercritical pressure (>10 kbar). Thin aluminum foil strip (~10 μm) sandwiched between two sapphire plates (~1 mm) is heated by an electrical current pulse for less than 1 μs, so that the Joule heat deposited into the sample achieves 4–6 the cohesion energy. Such experimental technique ensures sufficiently homogeneous heating and practically one-dimensional expansion of the foil strip. The current through the sample, the voltage drop across its length, and the pressure near the sample surface are measured. From the measured quantities, the electrical resistivity and pressure, both as functions of density and internal energy, are directly determined. Present results show that the dependence of the electrical resistivity of aluminum on internal energy along isochores acquires a negative slope at a density that is about three times lower than the standard solid density that indicates transition into a nonmetallic state. The equation of state relation obtained in this work evidences that this transition is continuous.

DOI: 10.1103/PhysRevB.75.064208 PACS number(s): 71.30.+h, 72.15.Cz, 64.30.+t, 52.25.−b

I. INTRODUCTION

In this paper, we report on the measurements of the electrical resistivity and some thermodynamic quantities on liquid aluminum undergoing a metal-nonmetal transition induced by expansion to low density. A great deal of attention has been given to such studies in the past to find out mechanisms of the transitions occurring in expanded metals. During the last decade, the interest to this problem has grown considerably. Partly that was caused by a progress in the calculations of electronic properties, ionic structure, and transport coefficients of expanded metals.

The calculation results have shown that in the electronic density of states of liquid mercury, there are well defined bands[1] without any indications for the localized states close to their edges as it was assumed earlier.[2] The transition of liquid mercury into a nonmetallic state starts when a gap between the 6*s* and 6*p* bands opens. Thus, the transition is well described by the conventional band model that predicts such behavior for any divalent metal.

For liquid aluminum, the quantum molecular-dynamics calculations of the electrical conductivity and thermodynamic functions were done in Refs. 3–8. The corresponding results demonstrate the onset of a metal-nonmetal transition when a gap separating the 3*s* and 3*p* levels forms about the Fermi energy.[4,5] However, it is still not clear what the role of temperature, the electron-electron interactions, and disorder is in that transition.

The dependences of the electrical conductivity on density and temperature calculated[4] were proven to be in a reasonable agreement with the experimental data,[9,10] though the data in Refs. 9 and 10 are not the results of direct measurements. The point is that the temperature and density were determined in those works using semiempirical equations of state of unknown accuracy. Thus, to explore the behavior of expanded aluminum in the metal-nonmetal transition range and to validate the calculation results[4–8] as well, direct measurements should be performed.

At the present, extensive experimental data in the metal-nonmetal transition range are available only for mercury, cesium, and in a smaller degree for other alkali metals. The measurements for metals with the higher critical-point parameters than those of mercury and alkali metals could not be fulfilled for lack of experimental techniques capable of performing accurate measurements at the temperatures of the order of 10 000 K and pressures of the order of 10 kbars, which correspond to the estimated critical temperatures and pressures for the majority of metals of the Periodic Table.

The exploding wire techniques[9,11] do provide such data on several metals with higher critical points, but the question about uncertainty of those data caused by the distributions of physical quantities across the wire samples still remains open. Special work devoted to this problem was done recently.[12,13] The distributions across tungsten wires were investigated by means of one-dimensional (1D) magneto hydrodynamics simulations of the exploding wire experiments. It was found that the uncertainties can be reduced to ~10% by choosing proper heating conditions but only at densities corresponding to six fold expansions and more. In the range of higher densities, the uncertainties reached 30% (see Refs. 12 and 13).

We have developed an experimental technique that provides sufficiently homogeneous heating of thin metal foils[10,14] and makes it possible the required temperature and pressure ranges to be achieved. For this technique, the temperature and density nonuniformities developed in the foil sample do not exceed 1%. The diagnostics we used earlier[10,14] were usual for this kind of experiments: only the current through the sample and voltage across it were measured. This set of measured quantities is not enough to obtain the electrical resistivity and the thermodynamic quantities characterizing the sample state without an auxiliary equation of state of the metal under investigation.

In the present study, in addition to the former diagnostics, we measure also the pressure close to the sample surface. This has permitted us to directly determine both the electrical

resistivity and pressure as functions of internal energy and density from the measured quantities. The density range investigated in this work extends from the standard solid density down to a value of six to nine times less. A typical pressure magnitude attained is 15–50 kbar that exceeds essentially the critical pressure of aluminum (that is, according to estimates, 2–5 kbar). As a result, the thermodynamic path representing the evolution of the sample state parameters during the heating process, for instance, in the pressure-density plane, does not intersect the liquid-gas equilibrium line. Hence, the sample always remains in a one-phase state (with the exception of a short time during which melting occurs).

II. EXPERIMENTAL SETUP AND DIAGNOSTICS

To perform the measurements on expanded aluminum, we utilize the pulse Joule heating technique proposed in Ref. 15 and then developed in the subsequent studies.[10,14] A thin metal foil is sandwiched between two relatively thick sapphire plates and rapidly heated by an electrical current pulse. The sapphire plates provide an inertia confinement for the hot metal sample by applying to it a sufficiently high dynamic pressure. Magnetohydrodynamic simulations of the heating dynamics have shown that under certain conditions (for certain geometrical dimensions of the experimental assembly, parameters of the discharge circuit producing the current pulse, etc.), the temperature and density distributions across the metal foil undergoing a five to ten-fold thermal expansion are practically uniform. Detailed description of the simulations and the estimates demonstrating the influence of different factors on the distribution of the physical quantities across the sample can be found elsewhere.[10,14]

The present experiments were carried out with aluminum foil strips, with a thickness of 16 μm, a width of 6 mm, and a length of about 10 mm. To perform the pressure measurements, we recorded the luminescence spectrum of ruby that was generated in a thin ruby plate. The plate (having a thickness of 380 μm, a width of 10 mm, and a length of 10 mm) together with the foil sample were sandwiched between two polished (of mirror quality) sapphire plates with a thickness of 1.6 or 3 mm, a width of 10 mm, and a length of 10 mm. The experimental assembly was carefully glued to exclude gaps (or voids) between its parts. Thin layers of epoxy glue (1–3 μm) completely filled the space between the aluminum foil and the plates. Such geometrical dimensions of the sample (small thickness compared to its length and width) and the confinement conditions ensure practically one-dimensional expansion of the sample material (it moves mainly along the direction perpendicular to the foil strip surface).[10,14]

The pulse heating of the foil samples was accomplished by discharging through them a 72μF capacitor bank charged to an initial voltage of 10–15 kV. The electrical circuit producing the current pulse and the diagnostics used to measure the voltage drop across the foil strip and the current through it are discussed in detail in Ref. 10. Typical temporal dependencies measured in the present experiments of the current through an aluminum foil strip, the voltage drop across its length, and the Joule heat released are shown in Fig. 1.

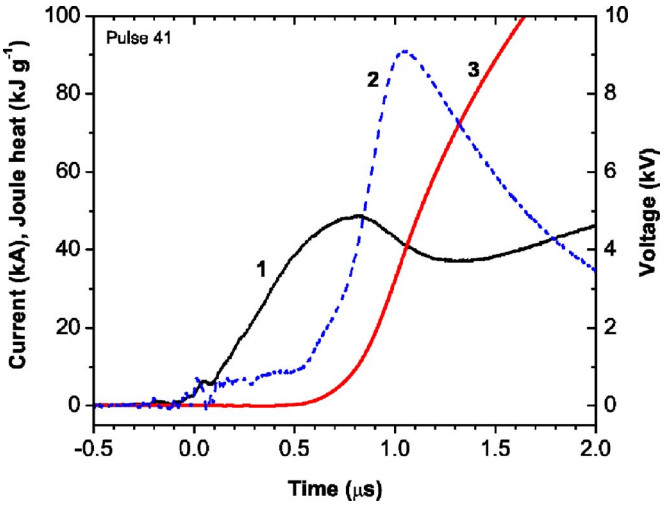

FIG. 1. (Color online) Temporal dependencies of the heating current (1), the voltage drop across the sample (2), and the specific Joule heat deposited into it (3) measured in this work, experiment 41.

The pressure measurements performed in this work are based on the ruby luminescence *R*-line shift technique that was introduced by Forman *et al.*[16] for diamond-anvil-cell measurements. Later, this technique was developed for the pressure measurements under the shock-wave hydrostatic loading, i.e., at pressures above the elastic limit of a solid material.[17] At last, the technique was developed to measure the stress in a solid sample under uniaxial shock-wave loading.[18] We apply this technique for the measurements of pressure under conditions of the pulse Joule heating when shock wave is usually absent and the sample density decreases with respect to its initial density. The ruby luminescence was exited by exposing an *a*-cut ruby plate (of optical quality) to a laser light. The ruby plate contained 0.7% Cr_2O_3 by weight and the crystal orientation was maintained within 1°. The ruby plate surface adjacent to the aluminum sample was covered by a dielectric mirror of 2 μm thickness with a reflectivity in the wavelength ranges of 500–550 nm and 650–700 nm of more than 95%. A pulsed neodymium-doped yttrium aluminum garnet laser (produced by Polyus, Russia) operated at 532 nm was used for pumping the luminescence. The laser pulse had a bell-like shape with a full width at half maximum of about 20 μs and an energy of 10 mJ. The laser light was guided by aspheric lenses and a quartz-polymer fiber of 400 μm in diameter on the ruby plate surface. The focused light spot on the surface had a diameter of about 200 μm. The luminescence light was captured by the same optical system, separated by a dichroic beam splitter from the pumping laser light, and focused on an entrance slit of an spectrograph (SpectraPro 500i, Acton Research) with a 1200 lines/mm grid. The Luminescence spectrum was dispersed over time by a streak camera (Optoscope by Optronis) operating at a streak speed of 100 ns/mm (measured at the luminescence screen). The total length of the streak record was about 1.6 μs.

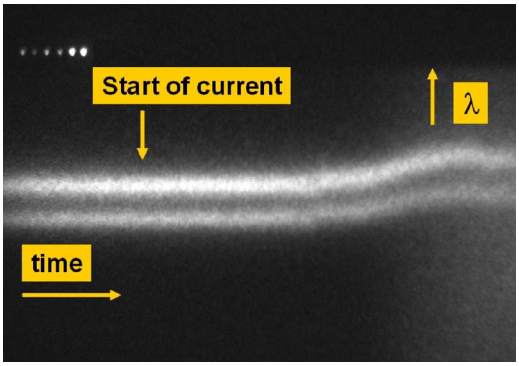

FIG. 2. (Color online) Streak image of the luminescence (R_1 and R_2 lines) generated in the ruby plate compressed by a dynamic pressure in the aluminum foil sample. The streak image is 1.6 μs long. At the left upper corner of the image there are time marks in 40 ns from the optical train pulse generator. The heating current starts at 140 ns after the last time mark.

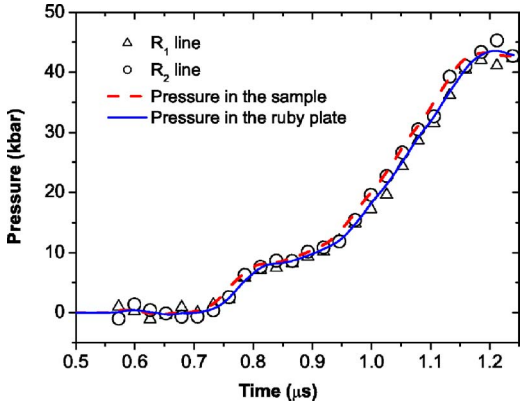

FIG. 3. (Color online) Pressure as a function of time measured in this work, experiment 35. The marks show the pressure values determined from the measured wavelength shifts for R_1 and R_2 lines. The black solid line represents the pressure at the middle of the ruby plate calculated for a given temporal dependence of the pressure at the metal-ruby interface (red dashed line).

III. PRESSURE MEASUREMENTS

A streak image of the luminescence generated in a ruby plate compressed by the expanding aluminum foil sample is presented in Fig. 2. The image shows the luminescence R line long before the heating current starts. As one can see, there is no remarkable influence of the magnetic field of the heating current on the shape and position of the lines. To prove this conclusion, the reader should take a look at Fig. 1, in which it is seen that the current reaches a value that is only by a factor of 2 smaller than the maximum value by 200–300 ns after the current starts. Till that time, the heating power remains very low and there is no remarkable heating of the sample (pressure is kept at a level less than 1 kbar). During this time, one does not observe any remarkable shifts of the luminescence lines in Fig. 2. That is why we concluded that there is no remarkable effect of the magnetic field. After the heating power increases sufficiently and the dynamic pressure reaches a level of 1 kbar or more, the lines are shifted and this can be clearly seen in Fig. 2. To determine the wavelength shifts from the luminescence spectra streak record, it was divided into 26 ns regions and for each of them an averaging was performed. The luminescence spectra averaged were approximated by the Lorentz function and the two R-line peaks were located. The luminescence spectrum at ambient pressure was recorded before each experiment, and the wavelength shifts were determined with respect to that reference.

To calculate the pressure from the measured wavelength shifts, we made use of the dependence of the wavelength shift on density change $\mu=\rho/\rho_0-1$ measured by Shen and Gupta for an a-cut ruby plate:[19]

$$\Delta\lambda = a\mu + b\mu^2 \tag{1}$$

(wavelength shifts are in nanometers, $a=116.3$ nm and $b=716.0$ nm for the R_1 line and $a=98.7$ nm and $b=0$ nm for the R_2 line), the Rankine-Hugoniot relations, and the relation between particle velocity u and shock velocity D for sapphire:[20]

$$D = 11.19 + 1.0u. \tag{2}$$

A temporal dependence of pressure measured in this work, experiment 35, is shown in Fig. 3. The systematic error in pressure caused by the difference between the measured pressure and that in the aluminum sample was estimated to be 1–2 kbar. When processing the measurements, data corrections were made for this systematic effect. To demonstrate that the correction was made properly, the pressure at the ruby plate surface adjacent to the sample and that at the middle of the plate are presented in this figure. The pressure at the middle of the ruby plate (that is assumed to be equal to the measured pressure obtained by averaging the two data sets for R_1 and R_2 lines) was calculated for a given temporal dependence of pressure at the ruby plate surface (that is assumed to be equal to the pressure in the aluminum sample). In these calculations, 1D equations of movement for the ruby plate and the adjacent sapphire plate were integrated numerically. The boundary conditions were posed at the metal-ruby interface (the pressure is a given function of time) and at the free surface of the sapphire plate (pressure is equal to 1 atm). As one can see the calculated values of pressure at the middle of the ruby plate are sufficiently close to the average value for the R_1 and R_2 line data.

The main contributions to the pressure measurement uncertainty give the systematic uncertainty in the coefficients of Eq. (1) and random error of the R-line peak position measurements (0.02 nm at ambient pressure). The streak speed was proven to be constant within 5%. This value was obtained using the time marks from optical train generator (GEC, Optronis). The system dispersion was determined as follows. The R-line positions at ambient pressure were recorded several times at three settings of the spectrograph wavelength selector in a 1 nm wavelength interval (this interval includes the maximum wavelength shift observed in these experiments). The average variation in the peak position was proven to be a linear function of the wavelength shift to within 3%. The separation between the R_1 and R_2 peaks was determined to be 1.4 nm with an error of less than

3%. The standard deviation of the data points presented in Fig. 3 from an average value did not exceed 6%. Taking into account all these uncertainties, the total uncertainty of the pressure measurements was estimated to be 12% at 10 kbar with monotonous decrease to 8% at 50 kbar.

IV. RESULTS

From the measured temporal dependence of pressure in the aluminum sample, its volume as a function of time was determined. The displacement of the metal-sapphire interface was calculated by solving the one-dimensional hydrodynamic task about movement of a piston into a medium in which the mechanical properties are known (sapphire in this case) and the pressure at the piston position is a given function of time. Throughout this paper, we neglect the difference in mechanical properties of ruby and sapphire. The equation of state of sapphire within the range of elastic strain ($P < 125$ kbar) is known with a high precision. In the case of isentropic flow, the equation of state (for uniaxial strain) can be written as a relation between pressure and density ρ as follows:

$$P = \frac{B}{n}\left[\left(\frac{\rho}{\rho_0}\right)^n - 1\right], \tag{3}$$

where ρ_0 is the normal density of sapphire and the coefficient B and the exponent n are assumed to be constant. The values of these parameters were found by fitting to the literature data on the mechanical properties of sapphire[20] ($\rho_0 = 3.985$ g/cm^3, $B = 499.0$ GPa, and $n = 3.0$).

For the time interval before the compression waves formed in the sapphire plates reflect from the free surfaces and come back to the sample, the displacement of the metal-sapphire interface can be calculated using a simple analytical formula. To derive it, let us assume first that the experimental assembly possesses symmetry about the plane passing through the middle of the foil strip parallel to the metal-sapphire interfaces. In this case, we may consider only the wave that propagates to the right. Let us direct the x axis of a coordinate system in that direction. Under such conditions, the Riemann invariant J_- is constant along the characteristic corresponding to the left-facing sound wave.[21] Using the equation of state [Eq. (3)], for the region inside the wave, one obtains

$$J_- = u - \frac{2c}{n-1}, \tag{4}$$

where u is the particle velocity and c is the longitudinal sound speed corresponding to the uniaxial compression. From Eq. (3), the sound speed can be easily determined as

$$c = c_0\left(\frac{\rho}{\rho_0}\right)^{(n-1)/2}, \tag{5}$$

where $c_0 = \sqrt{B/\rho_0}$. For the region where sapphire is in rest ($u = 0$), the Riemann invariant J_- has a constant value of

$$J_- = \frac{2c_0}{n-1}. \tag{6}$$

Substituting this value into the left-hand part of Eq. (4), we find the following relation between particle velocity and density:

$$u = \frac{2c_0}{n-1}\left[\left(\frac{\rho}{\rho_0}\right)^{(n-1)/2} - 1\right]. \tag{7}$$

At the metal-sapphire interface, the boundary condition is $u = U$, where U denotes the interface velocity. The interface displacement $\Delta X(t)$ at an instant of time t is determined by

$$\Delta X(t) = \int_0^t U(\tau)d\tau.$$

By expressing the density as a function of pressure from Eq. (3) and substituting that in Eq. (7), we finally find

$$\Delta X(t) = \frac{2c_0}{n-1}\int_0^t \left[\left(\frac{nP(\tau)}{B} + 1\right)^{(n-1)/2n} - 1\right]d\tau, \tag{8}$$

where $P(\tau)$ is the pressure at the metal-ruby interface.

For the later times, when the reflected waves disturb the sample movement, formula (8) is not valid. For present experiments with the sapphire plates of 3 mm in thickness, that happens at about 0.5 μs after the pressure in the sample begins to rise. This is a long enough period of time to reach the required expansions of the sample. Hence, in this case, formula (8) can be used for the whole time interval of the pressure measurements, but that was not the case for experiments with the thinner plates. For those experiments, the sample volume was calculated numerically. The numerical 1D hydrodynamic calculations were conducted taking into account both the actual asymmetry of the experimental assembly and the thin epoxy layers between its parts. That was done also to find out contributions of these factors to the pressure and the sample volume uncertainties. The analytic solution (8) was used to check accuracy of the numerical calculations.

Knowing the sample volume and pressure, one determines the work performed by the expanding aluminum sample on the sapphire plates and the fraction of the Joule heat imparted into the sample, resulting in its internal energy. The electrical resistivity σ^{-1} (σ denotes conductivity) was determined by

$$\sigma^{-1} = R(t)d(t)h/l, \tag{9}$$

where $R(t)$ is the sample resistance determined from the measured current and voltage records, $d(t)$ is the sample thickness, h and l are its width and length, correspondingly (both assumed to be constant). Thus, from the measured quantities, one may obtain the dependence of the electrical resistivity on the specific volume V and the specific internal energy E and a similar dependence for pressure, $P = P(V,E)$, that is often referred to as the caloric equation of state.

In this work, we report on the results obtained in five experiments. Two experiments (39 and 41) had almost identical parameters. The charging voltage was 15 kV and the

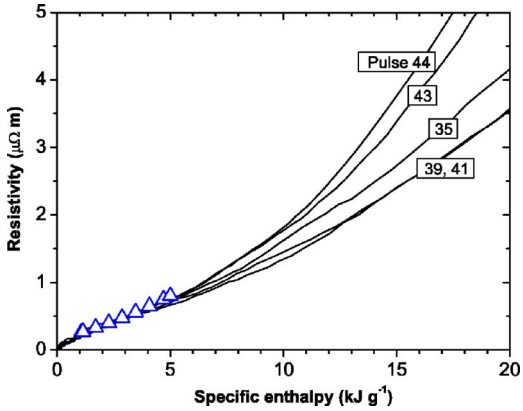

FIG. 4. (Color online) The electrical resistivity of expanded aluminum as a function of the specific enthalpy. The solid lines show this work measurement results, and the open triangles represent the data obtained under isobaric heating at 3 kbar (Ref. 22).

sapphire plates had a thickness of 3 mm. In these two experiments, the highest pressure was attained that resulted in the largest expansion of the aluminum sample for the time of measurements. Another pair of experiments (43 and 44) corresponds to a lower pressure level, and these experiments also had identical (one to another) parameters: the sapphire plates with a thickness of 1.6 mm were used and the capacitor bank was charged to an initial voltage of 10.3 kV. The fifth experiment (35) corresponds to an intermediate pressure and in that case the sapphire plates had a thickness of 3.0 mm and the capacitor bank was charged to 13.3 kV.

In Fig. 4, the dependences of the electrical resistivity versus the specific enthalpy measured in this work experiments are presented. The specific enthalpy W was calculated according to the formula $W=E+PV$. The data obtained under isobaric heating at 3 kbar (Ref. 22) are also shown for comparison. In Fig. 5, the dependences of the relative volume V/V_0 versus enthalpy are shown (V_0 is the specific volume of aluminum at standard conditions). As can be seen from these figures, our measurements agree well with the data of Ref. 22. It should be noted that the specific enthalpy values pre-

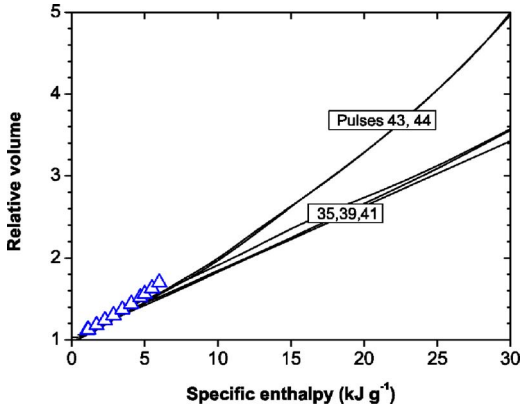

FIG. 5. (Color online) The relative volume of expanded aluminum plotted against the specific enthalpy. The solid lines correspond to the present experiments, and the open triangles are the data obtained under isobaric heating at 3 kbar (Ref. 22).

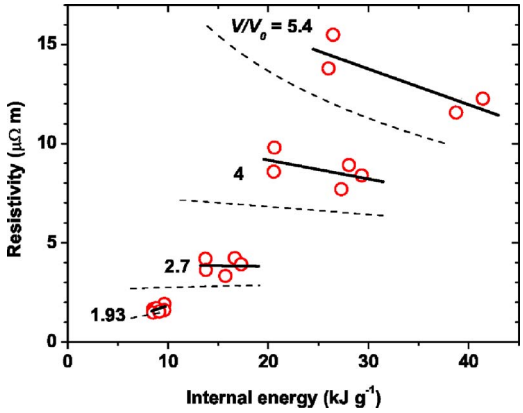

FIG. 6. (Color online) The electrical resistivity of aluminum vs the specific internal energy along four isochores in the metal-nonmetal transition range. The open circles are the present work values at the isochores $V/V_0=1.93$, 2.7, 4, and 5.4. The solid lines are linear fits of these data and the dashed lines are data of Ref. 10.

sented in Figs. 4 and 5 are, in fact, variations of enthalpy from its value at standard conditions in the solid state. The same belongs to the internal energy values presented in this paper. In our experiments, the heating was not isobaric and the pressure continuously increased in the enthalpy range shown in Figs. 4 and 5. At an enthalpy value of 5 kJ/g of this work, experiments 43 and 44, the pressure was within 7–8 kbar, and in experiments 39 and 41, it was 10–12 kbar. The effect of pressure can be clearly seen in Fig. 5, where our data demonstrate smaller relative volume values compared to those of Ref. 22.

The behavior of the electrical resistivity of expanded aluminum in the metal-nonmetal transition range is shown in Fig. 6. Four dependences of the resistivity on internal energy along isochores are presented. Our data obtained in Ref. 10 are also shown. It should be noted that the main conclusions made in Ref. 10 on the behavior of the electrical resistivity of aluminum in the metal-nonmetal transition range are confirmed in this work except for the absolute resistivity values along isochores, which differ by 20%–30%. That is assumed to be a result of the error in the equation of state model used in Ref. 10 to calculate the sample volume and temperature. Uncertainties in the present work data are as follows. The uncertainty in the resistivity values at all isochores is 6% and that in the specific internal energy is 15%.

As one can see, the slope of the dependences of the resistivity on internal energy along isochores in Fig. 6 changes its sign. It is positive for an isochore $V/V_0=1.93$. At a density that is 2.7 times lower than the standard solid density, the resistivity is practically constant, and at lower density, $V/V_0=4.0$, the slope becomes negative and remains so at $V/V_0=5.4$. There are no literature data to be compared directly with in this plane, but a very similar behavior for expanded liquid aluminum was predicted in the quantum molecular-dynamics calculations[4] for the electrical conductivity versus temperature along isochores.

In Fig. 7, pressure versus the specific internal energy along four isochores in the metal-nonmetal transition range is shown. The blue dashed lines represent dependencies obtained from the SESAME table 3720.[23] As one can see, our

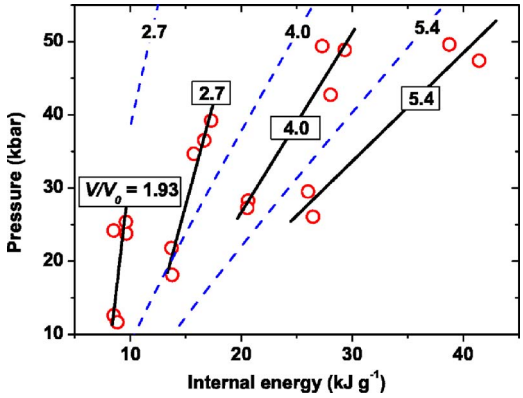

FIG. 7. (Color online) Pressure plotted against the specific internal energy along four isochores in the metal-nonmetal transition range. The red open circles correspond to the present work data at the isochores V/V_0=1.93, 2.7, 4, and 5.4. The black solid lines are linear fits of these data. The blue dashed lines are dependencies along three isochores obtained from the SESAME table 3720.

data demonstrate monotonic decrease in the slope of the dependence of pressure on the specific internal energy along isochores when density is lowered. The same behavior can be seen in Fig. 8, where the dependences of pressure versus relative volume for several constant internal energy values are presented. The corresponding dependences taken from the SESAME table 3720 demonstrate also a monotonic change in the partial derivatives of pressure; the reader should be reminded that the SESAME equation of state was constructed as a smooth interpolation of thermodynamic state functions between the condensed states and the ideal-gas states.

The relative volume values in our data were determined with an estimated uncertainty of 8% for expansion V/V_0 =2.7 and 12% for V/V_0=5.4 (at $P>25$ kbars). To compare our data directly with the results found in the literature (Refs. 5–8), we present in Figs. 9 and 10 the resistivity and pressure plotted against the specific internal energy at a relatively large expansion V/V_0=9. Only in experiments 39 and 41 were good quality luminescence spectra obtained at this expansion. In other experiments, this value was achieved for a longer time when the signal-to-noise ratio becomes too low to get representative data. The data reported in Refs. 8 and 11 are also shown in Fig. 9, though those data were originally presented as dependences of the resistivity versus temperature. As one can see in Fig. 10, for expansion V/V_0=9, the data taken from SESAME table 3720 are in good agreement with this work results. Hence, one may expect that the calculation of the internal energy by means of the SESAME table 3720 for this isochore does not produce large errors.

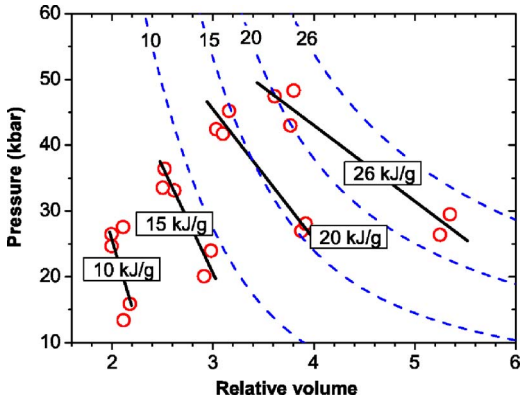

FIG. 8. (Color online) Pressure plotted against the relative volume at four fixed internal energy values. The red circles correspond to the present work data, the black solid lines are linear fits of these data, and the blue dashed lines are dependencies obtained from the SESAME table 3720.

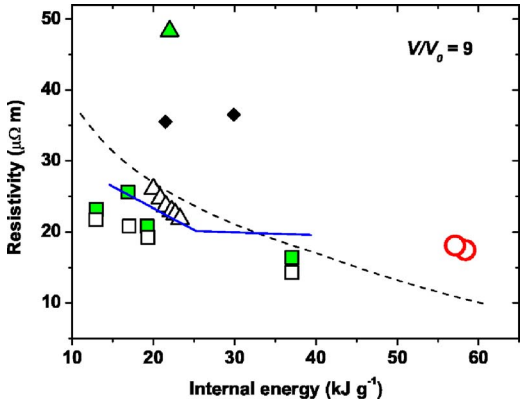

FIG. 9. (Color online) The electrical resistivity of aluminum vs the specific internal energy along isochore V/V_0=9.0. This work values (two red open circles) are compared with the experimental data of Ref. 5 (green solid triangle), calculation results of Ref. 5 (green solid squares), experimental data of Ref. 7 (open triangles), calculation results of Ref. 7 (open squares), experimental data of Ref. 11 (solid diamonds), and calculation results of Ref. 8 (solid blue line). The black dashed line shows data of Ref. 10.

V. ANALYSIS AND DISCUSSION

Our results show that the slope in the dependence of the electrical resistivity on internal energy along isochores

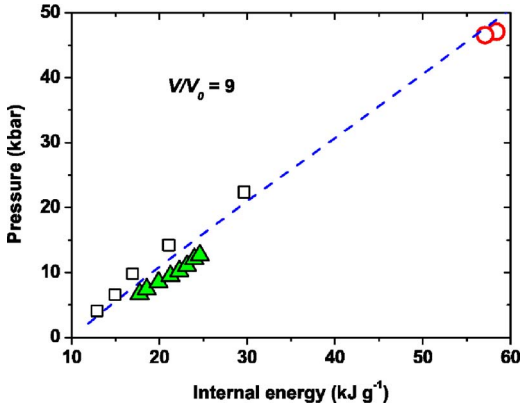

FIG. 10. (Color online) Pressure as a function of the specific internal energy along isochore V/V_0=9.0. The present work data (two red open circles) are compared with the experimental data of Ref. 6 (solid triangles), the calculation results of Ref. 6 (open squares), and the dependence obtained from the SESAME table 3720 (blue dashed line).

changes its sign at a density that is about three times less than the standard solid density (see Fig. 6). Since the constant volume heat capacity is positive, it follows that the corresponding dependence of the electrical resistivity on temperature also changes sign at this density. Does this behavior indicate the onset of a metal-nonmetal transition?

To answer this question, we first recall some facts from the observations of the metal-nonmetal transitions in different systems.[24] Measurements performed on alloys and compounds have shown that the positive temperature dependence of the resistivity becomes weaker or even changes sign in the strongly disordered limit. Those substances demonstrate the positive slope in a range of the resistivity $\sigma^{-1} < 1-2\ \mu\Omega\,\mathrm{m}$, and the slope becomes negative at higher values of σ^{-1}. On the other hand, for many metals and compounds, when temperature increases, the dependence of the resistivity on temperature becomes weak and then saturates, so that σ^{-1} reaches a maximum value of the order of $1.0\ \mu\Omega\,\mathrm{m}$. In both cases, the maximum value of the resistivity corresponds to the Ioffe-Regel limit, i.e., when the mean free path of the conducting electrons becomes comparable to the interionic separation. These facts suggest that the static (compositional) disorder and that due to temperature increase (dynamic disorder) produce a similar effect.[24] Thus, one may assume that there is a universal behavior of substances in the metal-nonmetal transition range, and, therefore, the measurements of the dependence of the resistivity on temperature along isochores even in the case of expanding liquid metals can be used for detecting the metal-nonmetal transition range.

In our experiments, we trace the evolution of the aluminum sample expanded under a supercritical pressure. We clearly see the moment when melting occurs and the sample passes into the liquid phase for which reliable literature data exist.[22] Our results are in a reasonable agreement with those data. We have found a positive slope in the dependence of the resistivity versus internal energy along isochore $V/V_0 = 1.93$ in the internal energy range that is very close to that of Ref. 22. The positive slope in the temperature dependence of resistivity is predicted by the diffraction theory for a trivalent liquid metal.[24] Thus, we conclude that at expansion $V/V_0 = 1.93$, aluminum is still on the metallic side of the metal-nonmetal transition.

Estimate show that the Ioffe-Regel criterion $\Lambda \geqslant d_{ii}$ is still valid at expansion $V/V_0 = 1.93$, where Λ is the mean free path of the conducting electrons and d_{ii} is the interionic separation. At expansion $V/V_0 = 2.7$, the criterion fails. At this expansion, σ becomes less than σ_{min}, where σ_{min} is the conductivity calculated according to the Drude formula

$$\sigma = \frac{n_e e^2 \Lambda}{\hbar k_F} \tag{11}$$

when one puts $\Lambda = d_{ii}$. Here, n_e is the valence electron number density, e is the electron charge, k_F is the Fermi wave vector, and $\hbar$ is the Plank constant. The electron number density is related to the ionic number density n_i by $n_e = z n_i$, where z is the number of the conducting electrons per ion (it was taken to be 3). The interionic separation was determined by the relation

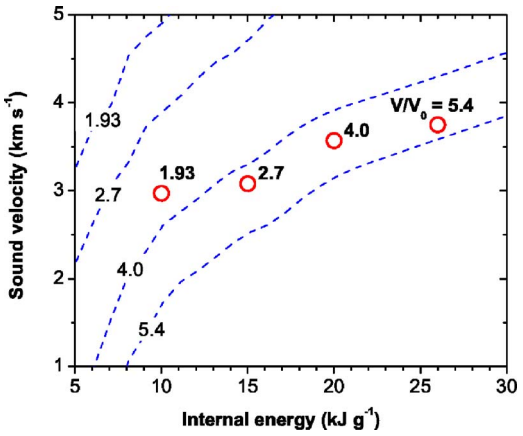

FIG. 11. (Color online) Sound velocity of expanded aluminum as a function of the specific internal energy at four fixed values of the relative volume. This work data (open red circles) are compared with the corresponding dependences taken from the SESAME table 3720 (dashed blue lines). The numbers indicate the values of the relative volume.

$$\frac{\pi}{6} d_{ii}^3 n_i = 0.63, \tag{12}$$

which expresses condition of dense random packing of hard spheres of diameter d_{ii}. The value of the resistivity $(\sigma_{min})^{-1}$ for $V/V_0 = 1.93$ calculated in this way is about $2\ \mu\Omega\,\mathrm{m}$. Hence, the estimate result is in agreement with the conclusion about the metallic behavior of expanded aluminum at $V/V_0 = 1.93$, since the corresponding resistivity values along the isochore are below $2\ \mu\Omega\,\mathrm{m}$. It should be noted also that the Fermi temperature for 1.93-fold expanded aluminum is about 90 000 K that is much larger than the temperature range in which the metal-nonmetal transition is detected. Thus, expanded aluminum at this density is still a strongly degenerate system like a good metal.

The metallization density can be derived also from the Herzfeld criterion that reads

$$\frac{4\pi}{3} \alpha n_i = 1, \tag{13}$$

where α is the atomic polarizability. For the measured polarizability value $\alpha = 6.8 \times 10^{-24}\ \mathrm{cm}^3$ (Ref. 25), one obtains the relative volume at the metallization point $V/V_0 = 1.7$ that seems to be contradicting to the present results.

At sufficiently high temperatures and pressures, continuous transition of expanded liquid metal into a gaseous dielectric state is expected.[26] This point of view is supported by some observations made in the present work. The first is the monotonic change in the equation of state dependences across the transition range shown in Figs. 7 and 8. The relative volume and resistivity also demonstrate smooth variations with enthalpy (see Figs. 4 and 5). Besides that, the sound velocity values calculated from the equation of state data obtained in this work and shown in Fig. 11 also provide evidence of a continuous transition. The sound velocity c_s was determined using the following relation:

$$c_s = V\sqrt{-\left(\frac{\partial P}{\partial V}\right)_E + P\left(\frac{\partial P}{\partial E}\right)_V}. \quad (14)$$

The states at which the sound velocity values presented in Fig. 11 were calculated turned out to be very close to an isobar of 28 kbar. Thus, the sound velocity of expanded aluminum demonstrates no abrupt changes as, e.g., in the case of a liquid-vapor phase transition. Liquid aluminum at the melting point has a sound velocity value of 4.7 km/s.[27] The value of about 3 km/s obtained in this work at $V/V_0=1.93$ seems to be consistent with the data obtained for liquid lead.[28] In that work, the sound velocity falls by a factor of 2 when density decreases by 80% with respect to the melting point density. Interestingly, the sound velocity of mercury[29] shows only a slight increase with temperature along a supercritical isobar at expansions $V/V_0>2$ that is very similar to the present results.

VI. CONCLUSIONS

We have performed direct measurements of the electrical resistivity and the state functions on expanded aluminum in the metal-nonmetal transition range. We observed change of sign in slope of the dependence of the resistivity on internal energy along isochores that, in our opinion, indicates transition of aluminum into a nonmetallic state. The equation of state relation obtained in this work evidences that this transition is continuous at pressures above 15 kbars.

ACKNOWLEDGMENTS

We thank M. B. Agranat for providing us the Optoscope streak camera. This work was performed under the financial support of Presidium of Russian Academy of Sciences in the framework of the program "Thermophysics and mechanics of high-powered energetic actions" and the Russian Foundation for Basic Research (Grant No. 06-08-00304-a).

*Electronic address: savlab@iht.mpei.ac.ru

[1] G. Kresse and J. Hafner, Phys. Rev. B **47**, R558 (1993).
[2] N. Mott, Rep. Prog. Phys. **47**, 909 (1984).
[3] P. L. Silvestrelli, Phys. Rev. B **60**, 16382 (1999).
[4] M. P. Desjarlais, J. D. Kress, and L. A. Collins, Phys. Rev. E **66**, 025401(R) (2002).
[5] V. Recoules, P. Renaudin, J. Clérouin, P. Noiret, and G. Zéerah, Phys. Rev. E **66**, 056412 (2002).
[6] P. Renaudin, C. Blancard, J. Clérouin, G. Faussurier, P. Noiret, and V. Recoules, Phys. Rev. Lett. **91**, 075002 (2003).
[7] V. Recoules, J. Clérouin, P. Renaudin, P. Noiret, and G. Zérah, J. Phys. A **36**, 6033 (2003).
[8] G. Faussurier, C. Blancard, P. Renaudin, and P. L. Silvestrelli, Phys. Rev. B **73**, 075106 (2006).
[9] A. W. DeSilva and J. D. Katsouros, Phys. Rev. E **57**, 5945 (1998).
[10] V. N. Korobenko, A. D. Rakhel, A. I. Savvatimski, and V. E. Fortov, Phys. Rev. B **71**, 014208 (2005).
[11] I. Krisch and H.-J. Kunze, Phys. Rev. E **58**, 6557 (1998).
[12] A. W. DeSilva and A. D. Rakhel, Int. J. Thermophys. **26**, 1137 (2005).
[13] A. W. DeSilva and A. D. Rakhel, Contrib. Plasma Phys. **45**, 237 (2005).
[14] V. N. Korobenko, A. D. Rakhel, A. I. Savvatimskiy, and V. E. Fortov, Plasma Phys. Rep. **28**, 1008 (2002).
[15] V. N. Korobenko and A. D. Rakhel, Int. J. Thermophys. **20**, 1259 (1999).
[16] R. A. Forman, G. J. Piermarini, J. D. Barnett, and S. Block, Science **176**, 284 (1972).
[17] H. K. Mao, P. M. Bell, J. W. Shaner, and D. J. Steinberg, J. Appl. Phys. **49**, 3276 (1978).
[18] P. D. Horn and Y. M. Gupta, Appl. Phys. Lett. **49**, 856 (1986).
[19] X. A. Shen and Y. M. Gupta, Phys. Rev. B **48**, 2929 (1993).
[20] L. M. Barker and R. E. Hollenbach, J. Appl. Phys. **41**, 4208 (1970).
[21] L. D. Landau and E. M. Lifshitz, *Fluid Mechanics* (Pergamon, Oxford, 1992).
[22] G. R. Gathers, Int. J. Thermophys. **4**, 209 (1983).
[23] The SESAME table 3720 was sent us from the SESAME Library at our request by S. D. Crockett in February, 2004. Description of the approach used in constructing the SESAME equation of state can be found in S. P. Lyon and J. D. Johnsn, LANL Report LA-CP-98–100 (unpublished).
[24] V. F. Gantmakher, *Electrons in Disordered Media* (Fizmatlit, Moscow, 2003) (in Russian).
[25] Paolo Milani, I. Moullet, and Walt A. de Heer, Phys. Rev. A **42**, 5150 (1990).
[26] Ya. B. Zel'dovich and L. D. Landau, Zh. Eksp. Teor. Fiz. **14**, 32 (1944).
[27] *Physical Quantities: Handbook*, edited by I. S. Grigorev and E. Z. Meylikhov (Energoatomizdat, Moscow, 1991).
[28] R. S. Hixson, M. A. Winkler, and J. W. Shaner, Int. J. Thermophys. **7**, 161 (1986).
[29] V. F. Kozhevnikov, D. I. Arnold, and S. P. Naurzakov, Int. J. Thermophys. **16**, 619 (1995).